IEEE Access
Multidisciplinary | Rapid Review | Open Access Journal

Received 30 May 2023, accepted 8 June 2023, date of publication 11 July 2023, date of current version 19 July 2023.

Digital Object Identifier 10.1109/ACCESS.2023.3294230

RESEARCH ARTICLE

Automated Red Palm Weevil Detection Using Gorilla Troops Optimizer With Deep Learning Model

AMANI ABDULRAHMAN ALBRAIKAN[1], MAJDI KHALID[2], NUHA ALRUWAIS[3], TAWFIQ HASANIN[4], ASHIT KUMAR DUTTA[5], HEBA MOHSEN[6], MOHAMMED RIZWANULLAH[7], AND SARA SAADELDEEN IBRAHIM[7]

[1]Department of Information Systems, College of Computer and Information Sciences, Princess Nourah bint Abdulrahman University, Riyadh 11671, Saudi Arabia
[2]Department of Computer Science, College of Computers and Information Systems, Umm Al-Qura University, Makkah 21955, Saudi Arabia
[3]Department of Computer Science and Engineering, College of Applied Studies and Community Services, King Saud University, Riyadh 11495, Saudi Arabia
[4]Department of Information Systems, Faculty of Computing and Information Technology, King Abdulaziz University, Jeddah 21589, Saudi Arabia
[5]Department of Computer Science and Information Systems, College of Applied Sciences, AlMaarefa University, Riyadh 13713, Saudi Arabia
[6]Department of Computer Science, Faculty of Computers and Information Technology, Future University in Egypt, New Cairo 11835, Egypt
[7]Department of Computer and Self Development, Preparatory Year Deanship, Prince Sattam bin Abdulaziz University, Al-Kharj 16278, Saudi Arabia

Corresponding author: Mohammed Rizwanullah (r.mohammed@psau.edu.sa)

Princess Nourah bint Abdulrahman University Researchers Supporting Project number (PNURSP2023R191), Princess Nourah bint Abdulrahman University, Riyadh, Saudi Arabia. Research Supporting Project number (RSPD2023R608), King Saud University, Riyadh, Saudi Arabia. This study is partially funded by the Future University in Egypt (FUE). This study is supported via funding from Prince Sattam bin Abdulaziz University project number (PSAU/2023/R/1444).

ABSTRACT Red palm weevil (RPW) is a pest that can cause severe damage to plantations and affects palm trees. Classical approaches to detection depend on visual analysis, which is inaccurate and time-consuming. Hence, deep learning techniques emerge as a potential solution used for automating the process of detection and presenting efficient and precise results. The initial detection of the RPW remains a difficult task for good production as the identification will protect palm trees infected from the RPW. So advanced technologies like artificial intelligence (AI) and computer vision (CV) can be used in preventing the spread of the RPW on palm trees. Various scholars still working on identifying a precise method for the classification, identification, and localization of the RPW pest. This article develops an automated Red Palm Weevil Detection using Gorilla Troops Optimizer with Deep Learning (RPWD-GTODL) method. The goal of the presented RPWD-GTODL approach lies in the accurate detection and localization of the RPW effectually. To accomplish this, the presented RPWD-GTODL technique initially uses the Gabor filtering (GF) technique to pre-process the images. For RPW detection, the RPWD-GTODL technique uses a Mask RCNN object detector with MobileNetv2 as a backbone network. Moreover, the detection performance of the RPWD-GTODL technique can be boosted by the design of the GTO algorithm for the hyperparameter selection of the MobileNetv2 model. The performance validation of the RPWD-GTODL technique is tested using the RPW dataset and the results demonstrate the enhanced performance on RPW detection process with maximum accuracy of 99.27%.

INDEX TERMS Computer vision, red palm weevil, Gabor filtering, deep learning, gorilla troops optimizer.

I. INTRODUCTION

The Date Palm (DP) is a greatly valued fruit yield which gives healthful food safety to millions of inhabitants around the globe [1]. It is also regarded as a significant resource for exporting income for limited scalers of the countryside global-wise. Regrettably, the manufacturing of date and its marketing are under threat due to the Red Palm Weevil (RPW), as well called ''Rhynchophorus Ferrugineus'' [2]. RPW was a coleopteran snout bug that is regarded as the sole greatest damaging bug of palm trees. Soft and adolescent trees that are younger than twenty years which signifies

The associate editor coordinating the review of this manuscript and approving it for publication was Gustavo Olague.

approximately fifty percent of the overall harvested DP trees are weak since RPW usually aims at them [3]. Alongside DPs, RPW also damages oil, coconut, and decorative palms. Over the last few years, RPW is discovered in greater than sixty nations encompassing the Middle East, Mediterranean region, North Africa, and portions of Central USA, among others [4]. This pestilence has devastated several palm farmhouses worldwide resulting in many financial losses in the shape of manufacturing deprivation or epidemic-control expenses. In the initial phase of the plague, DP trees can be cured with biochemical handlings [5]. Still, DP vegetation only depicts visual suffering symptoms in an extreme phase of the plague, where it is hard to rescue the vegetation. Several methods are stated in the works for the primary identification of RPW [6]. Few identification techniques like x-ray-founded tomography and trained dogs were precise; still, they fall short in the possibility of large-scale farmhouses due to their sluggish scanning procedures.

Significantly, the initial identification of palm tree plague may rescue trees from permanent harm [7]. In those initial phases, regulating procedures could be employed, most prevalently by the usage of pesticides. Hence, to abolish pestilence effectively, an exact charting of pestilence hot zones is greatly desirable, particularly of privately implanted palm trees, whose positions are not recorded formally. Over the past two decades, several RPW identification procedures were suggested. Applied AI methods and procedures in the area of farming have turned out to be a current fashion in the context of precise farming [8]. Also, these intellectual procedures have been prosperously incorporated in farming applications in prior studies, for example, the detection of apple-leaf ailments, categorization of bugs, and cultivating machinelike schemes. Nonetheless, the large database and huge machinery sources like Graphical Processing Units (GPUs) are the main needs of conventional DL methods needed to perform the training stage [9]. These needs are not always accessible to the end-users or developers. Hence, employing transfer learning procedures offer a better resolution for smart applications with restricted database and machinery sources [10]. They rely on transporting the information from a like duty to another duty by employing a similar pre-qualified prototype at less computation expense.

This article develops Automated Red Palm Weevil Detection using Gorilla Troops Optimizer with Deep Learning (RPWD-GTODL) model. The presented RPWD-GTODL technique initially uses the Gabor filtering (GF) technique to pre-process the images. For RPW detection, the RPWD-GTODL technique uses a Mask RCNN object detector with MobileNetv2 as a backbone network. Moreover, the detection performance of the RPWD-GTODL technique can be boosted by the design of the GTO algorithm for the hyperparameter selection of the MobileNetv2 model. The performance validation of the RPWD-GTODL technique is tested using the RPW dataset and the outcomes are studied in terms of different measures.

II. RELATED WORKS

Alsanea et al. [11] designed a method using a DL technique for discriminating and identifying the RPW and other insects in palm tree habitats. Here, a region-based CNN (R-CNN) technique has been adopted to discover the RPW location in an image by constituting bounding boxes near the images. For the extraction of the features to enclose with bounding boxes—the selection target, A CNN method was implemented. As well, such attributes have been sent through the regression and classification layers for determining the RPW with a higher level of precision and to place its coordinates. Kagan et al. [12] introduced an innovative method for surveillance of RPW-infested palm trees using existing DL techniques, with street-level and aerial image data.

In [13], the author presented an IoT-based smart palm monitoring prototype as a proof-of-concept that (1) contribute to the prompt recognition of PRW infestation and 2) allowed the monitoring of palms remotely through smart agriculture sensors. Users can use mobile apps or the web to communicate with palm farms and assist them in the timely recognition of likely infestations. The author exploited an industrial-level IoT platform to interface between the user layer and the sensor layer. In [14], the authors developed the first region-wide spatial inventory of Phoenix canariensis (canary palm) and Phoenix dactylifera (date palm trees), depending on remote images. CNN-based DL architecture was executed to create a detection method with the potential of classifying and locating individual palm trees from aerial high-resolution RGB imagery. Rhinane et al. [15] target the experimentation of the U-Net DNN technique for identifying individual date palm tree crowns from high spatial resolution images. This U-Net technique has been executed through Keras and Tensor-Flow.

Al-Megren et al. [16] offer an innovative autonomous bio-inspired technique for the efficient allocation of tasks among many UAVs in DAT missions. The performance of this devised technique was benchmarked against 2 long-standing multi-UAV task allocation paradigms: auction-based heuristics and opportunistic task allocation, which can be tested in the DAT mission for performance assessment. Karar et al. [17] introduced a method for identifying RPW larvae called an IoT-based sound detection technique for protecting date palm trees in the initial stage of infestation. The presented detection mechanism depends on a technique that serves as a recent DL classifier called a modified mixed depthwise convolutional network (MixConvNet). With the presented MixConvNet technique, the public TreeVibes data containing short audio recordings of feeding or moving RPW was effectively assessed and tested.

Mao et al. [18] establish integrating ML and fiber optic distributed acoustic sensing (DAS) as solution to detect the RPW from the larvae step. A single fiber optic cable will probably monitor 100 trees. Parvathy et al. [19] examines a Convolutional AE (CAE) based DL approach for detection of RPW acoustic emissions in other related noise. Mel spectrogram of acoustic instances can be selected as extraction feature for

the presented technique. The aimed of CAE can be trained utilizing Mel spectrogram image of RPW acoustic actions that can be considered as normal sample. The authors [20] introduces a ML approach dependent upon image processing for simply detect these insect species for people who does not recognize them. A fundamental idea of presented analysis is establish a NN technique, which is utilize image processing for identifying RPW and separate it from other insects found in palm tree habitats.

For the management and control of the RPWs, the existing models initially identify the occurrence of RPWs. include first detecting the presence of RPWs. These approaches have been modified to provide more accurate insect identification results in real-time in place of a lack of manual identification methods for entomologists. Several research works have focused on the development of accurate RPW detection techniques. Though few DL-based RPW detection models exist in the literature, they have not addressed the hyperparameter tuning process. None of the existing work has utilized a hyperparameter-tuned DL model for the RPW detection process. Diverse hyperparameters have a significant impact on the efficiency of the CNN model. Particularly, hyperparameters such as epoch count, batch size, and learning rate selection are essential to attain effectual outcomes. Since the trial and error method for hyperparameter tuning is a tedious and erroneous process, metaheuristic algorithms can be applied. Therefore, in this work, we employ the GTO algorithm for the parameter selection of the MobileNetv2 model.

III. THE PROPOSED MODEL

In this article, we have developed a new RPWD-GTODL technique for the accurate detection of the RPW and thereby improving the date tree productivity. The presented RPWD-GTODL technique exploited the computer vision (CV), DL, and parameter tuning concepts to accomplish automated detection performance. It follows a three-stage process: GF-based noise removal, MaskRCNN-based detection, and GTO-based hyperparameter tuning. Fig. 1 represents the overall flow of the RPWD-GTODL approach.

A. PRE-PROCESSING

At the primary stage, the input images are initially pre-processed by the use of the GF technique. It is a type of linear filtering that was planned for detecting particular spatial frequency and orientation features from the image [21]. This filtering can be dependent upon the Gabor function which is a Gaussian function modified by a sinusoidal wave. GF has extremely utilized in image processing and CV tasks like extraction features, edge detection, and texture analysis. It is utilized for extracting features, which are complex to capture utilizing other typical image processing systems. It operates by convolving the input image with a group of Gabor functions, every of which has a distinct orientation and spatial frequency. The resultant output is a group of filtering images, every capturing a particular feature of the

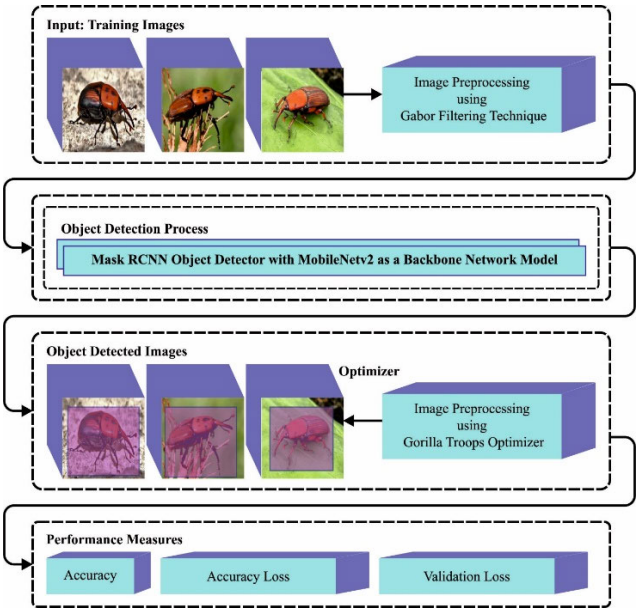

FIGURE 1. The overall flow of the RPWD-GTODL approach.

novel image. It provides major benefits to other linear filters namely the capability to capture either spatial or frequency information concurrently. This creates the appropriate image processing tasks but either low-level or high-level features can be needed.

B. DESIGN OF MASK RCNN-BASED RPW DETECTION

For accurate detection of RPW, the RPWD-GTODL technique uses the Mask RCNN model. Mask RCNN network is mainly composed of: Regional Suggestion Network (RPN), MobileNetv2 and Feature Pyramid Network (FPN), mask predictive branch, ROI Align, and full connection layer to accomplish the classification and regression [22]. MobileNetv2 is used to balance the speed and recognition performance during the process of testing and training. The initial layer of MobileNetv2 is applied for processing input images while layers 2-5 are encompassed by a basic residual module named bottleneck. The amount of bottleneck in layers 2-5 is 3, 4, 6, and 3 in sequence, and the bottleneck structure (initial bottleneck of layer 2). After, the sampled feature map $\{C_2, C_3, C_4, C_5\}$ is transported to FPN for upsampling and multiscale fusion to achieve $\{P_2, P_3, P_4, P_5\}$ that has high-level semantic and low-level contour data. The computation equation of the abovementioned process is given below:

$$P_5 = Conv_{1\times1}(C_5) \tag{1}$$

$$P_i = Conv_{1\times1}(C_i) \oplus f_{Up} \cdot (P_{i+1}), i \in \{2, 3, 4\} \tag{2}$$

In Eq. (1) and (2), P_i illustrates the feature map through FPN feature fusion of C_i, $Conv_{1\times1}$ characterize convolution using 1×1 kernels, C_j shows the feature map extracted from layer i, $\oplus$ signifies the addition operator of corresponding components, and f_{up} denotes the up-sampling. The $P_1 - P_5$ is convolved using $a3 \times 3$ kernel decreasing the

aliasing effect of up-sampling, and then transported to two branches of RPN. One branch is applied for judging the foreground or background, and connected with the softmax function for dual classification; another branch performs bounding box regression that produces an anchor with an aspect ratio at every pixel of feature in every layer, and the aspect ratio is set as [0.5, 1, 2]. Meanwhile, the size of features in FPN is not the same, the anchor area scale is set as $[32^2, 64^2, 128^2, 256^2, 512^2]$, viz., the size of the anchor is defined by the located layer. Afterwards traversing each pixel, Non-Maximum Suppression (NMS) is adopted for retaining anchor with higher confidence and getting proposals for candidate regions. In Fast RCNN, the ROI Pooling will pool the respective area into the fixed size in the feature map based on the position coordinate of the proposal, to enable the classification and regression process. Since the position of the proposal can be attained by regression, their coordinate was generally not an integer. But the proposal would be quantized two times by ROI Pooling to integer value resulting in obvious error. ROI Align exploits bilinear interpolation rather than quantization to evaluate the pixel value of the fixed four locations in every unit. Consequently, it effectively takes maximal pooling operation to increase the performance of output and make the model well-suited for the detection of smaller objects. Furthermore, Mask RCNN add a Fully Convolutional Network (FCN) that has the exact mask of input images for any size through operations namely step-hopping, convolutional and deconvolution structure to accomplish pixel level instance segmentation.

1) BACKBONE NETWORK

As a backbone network, the MobileNetV2 model is developed. The primary objective for adopting this model relies on its strength to comply with its design to be focused more on mobile applications [23], computational costs, and reducing memory usage. It should be pointed out that the model has around initially 1000 nodes in its classification layer. Nonetheless, to make it matchable with the given issue, it is appropriate to set the number of nodes in the classification layer. To enhance the reliability, a customized head, having 5 dissimilar layers was added to the base model of MobileNetV2 by substituting the classification layer. The customized head has (i) flatten layer, (ii) an average pooling layer, (iii) a softmax layer, (iv) a dense layer, and (v) a dropout layer. It should be noted that the size of the average pooling layer was set to (7×7). In the flattened layer, the flattened neuron was fed to the dense layer using the activation function being ReLu. This can be proceeded by setting the dropout layer probability with the value of 0.5 and the addition of 40 different nodes within the classifier layer of the model. These changes have generated a better version of the MobileNetV2 model bearing 40 nodes in its latter (classification) layer; this was a befitting and optimal method for the given issue.

2) LOSS FUNCTIONS

Mask RCNN applied a multi-task loss function which combines the loss of segmentation, classification and localization mask as given in the following [24].

$$L = L_{cls} + L_{bbox} + L_{mask} \tag{3}$$

In Eq. (3), L_{cls} and L_{bbox} are similar to Fast RCNN. The added mask L_{mask} showed in Eq. (4). Since the average binary cross-entropy involves only *kth* mask when the region is connected with the ground truth class k.

$$L_{m(xsk} = -\frac{1}{m^2} \sum_{lsi,jsm} y_{ij} \log \hat{y}_{ij}^{k} + \left(1 - y_{ij}\right) \log \left(1 - \hat{y}_{ij}^{k}\right) \tag{4}$$

In Eq. (4), the mask branch produces a mask of dimension $m * m$ for RoI and class y_{ij} and k, $\hat{y}$, ij is cell (i, j) labels of the true mask and the forecasted value correspondingly.

3) TRAINING

Mask RCNN needs a considerable amount of annotated datasets for training to mask the over-fitting. To resolve the problems of constraint annotated data in cluttered environments in robot applications, a transfer learning with the pre-trained network weight of the ResNet50 architecture was adopted and trained successfully with the coco data. We applied the pretrained ResNet50 and finetuned the network weight to the Coco data. Then, apply 30 epochs with a learning rate of 0.001. Then, different augmentation techniques are used namely vertical flip, horizontal flip, image translation, and image rotation to expand the training dataset. One can observe that this domain-specific fine tuning enables better learning network weight for the higher capability CNN for coco data.

C. HYPERPARAMETER TUNING USING GTO ALGORITHM

To enhance the detection performance, the RPWD-GTODL technique uses the GTO algorithm as a hyperparameter optimizer. The artificial GTO technique is a metaheuristic method inspired by the social behaviours of the gorilla [25]. The gorilla is the strongest and largest primate in the world nowadays. Every group is headed by the adult male gorilla which has a stronger sense of territory since the hair on the back of some gorilla members is white, this gorilla is also named Silverback gorilla. Fig. 2 represents the steps involved in the GTO algorithm.

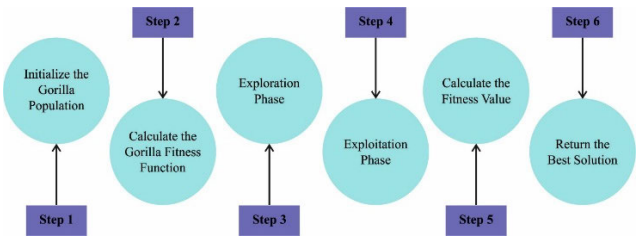

FIGURE 2. Steps involved in the GTO algorithm.

1) EXPLORATION STAGE

The three strategies in the exploration phase can be formulated in Eq. (5), where p represents the variables ranging from zero to one which controls the migration strategy of an unknown location. If $rand < p$, then the present position of the gorilla will move to an unknown location. This permits the GTO method to accurately track the whole problem space, making the distribution of solutions more comprehensive and scattered. On the other hand, if $rand \geq p$, two other strategies will be chosen. Next, if $rand \geq 0.5$, then gorillas migrate to other gorillas. These mechanisms make the present solution nearer to other solutions and enhance the exploration performance of GTO. If $rand < 0.5$, the gorilla will move to the known location. This improves the capability of the GTO to jump out of the local optimum solution.:

$$GX\,(t+1) = \begin{Bmatrix} (UB - LB) \times r_1 + LB, rand < p \\ (r_2 - C) \times X_r(t) + L \times H, rand \geq 0.5 \\ X(t) - L \times (L \times (X(t) - GX(t))) \\ +r_3 \times (X(t) - GX_r(t)), rand < 0.5\}' rand \geq p \end{Bmatrix} \quad (5)$$

In Eq. (5), the location vector dimension can be determined by the problem dimension. $GX(t+1)$ characterizes the location vector of the gorilla at the following iteration and $X(t)$ signifies the present location of the gorilla. r_1, r_2, r_3, and $rand$ represent random numbers between 0 and 1 generated with the standard distribution. The upper and lower boundaries are formulated as UB and $LB.X_r$ and GX_r show the location vector of selected gorillas randomly. The formula for evaluating, L, and H in Eq. (5) can be given as:

$$C = F \times \left(1 - \frac{t}{\text{Max}It}\right) \quad (6)$$

In Eq. (6), t signifies the existing amount of iterations and $Ma\chi It$ shows the maximal amount of iterations. Initially, the values of C have a larger change in the earlier phase and a smaller change in the later phase. This makes the earlier phase have great randomness to enlarge the range of exploration, and in the last phase, it becomes too small to attain the effects of quick convergence as follows:

$$F = \cos(2 \times r_4) + 1 \quad (7)$$

In Eq. (7), r_4 denotes the random integer within [0, 1] at a standard distribution to safeguard the randomness of the search that is conducive to finding the global optimum solution. L denotes variables that simulate the leadership of silverback gorillas that can be evaluated by the succeeding formula:

$$L = C \times l \quad (8)$$

In Eq. (8), l denotes the random integer within $[-1, 1]$ generated with the standard distribution. Silverback gorilla makes mistakes to find food or manage groups due to their lack of experience. Thus, they could attain extreme stability and reliable experience under the guidance of leaders. Simultaneously, Eq. (8) is used for simulating the leadership of the silverback gorilla. In the meantime, H in Eq. (5) is evaluated by Eq. (9). The Z in Eq. (9) is evaluated by Eq. (10), where Z refers to the random number in the problem dimension and the ranges of $-C, C$.

$$H = Z \times X(t) \quad (9)$$

$$Z = [-C, C] \quad (10)$$

In the exploration stage, the fitness value of GX and X is evaluated at the end. If the fitness values of $GX(t)$ are lesser than the fitness values of (t), then the location of $GX(t)$ replaces the location of $X(t)$.

2) EXPLOITATION STAGE

Silverback gorillas and other gorillas are best suited to implement their duty when young. Simultaneously, male gorilla prefers to follow silverback gorilla. Furthermore, every gorilla influences other gorillas. In other words, the present individual location solution of the gorilla follows the optimum solution of the silverback gorilla. They influence one another, and every solution affects other solutions. When $C \geq W$, then the policy would be performed. These behaviours are simulated by Eq. (11):

$$GX\,(t+1) = L \times M \times (X\,(t) - X_{silverbak}) + X\,(t) \quad (11)$$

where $X_{Silverback}$ characterizes the optimum solution, and M is evaluated using the following expression:

$$M = \left(\left| \frac{1}{N} \sum_{i=1}^{N} GX_i\,(t) \right|^g \right)^{\frac{1}{g}} \quad (12)$$

In Eq. (12), $GX(t)$ represents the vector location of every candidate gorilla. The location vector dimension can be determined by the problem dimension, N shows the overall amount of gorillas, and g is evaluated by Eq. (13):

$$g = 2^L \quad (13)$$

The main behaviour of adolescent gorillas is to compete with other gorilla members for the opposite sex. This type of competition can be represented by being intense, lasting, and capable of influencing other gorillas. The competition between them characterizes the mutual influence of solutions. The optimal solution for silverback gorillas moves to the location of other solutions, thus affecting the existing solution to the specific range and finding the best solution. These behaviours are simulated by the following expression:

$$GX\,(t) = X_{silverback} - (X_{silverback} \times Q - X\,(t) \times Q) \times A \quad (14)$$

$$Q = 2 \times r_5 - 1 \quad (15)$$

$$A = \beta \times E \quad (16)$$

$$E = \begin{cases} N_1, rand \geq 0.5 \\ N_2, rand < 0.5 \end{cases} \quad (17)$$

where A represents the coefficient vector used for stimulating the degree of competition, Q refers to the competition intensity of the simulated gorilla, r_5 denotes the random integer within [0, 1] at a standard distribution, E is used for stimulating the impacts of violence on the solution dimension, β shows the parameter set beforehand the optimization process, and *Rand* denotes the random integer within [0,1]. If $rand \geq 0.5$, E is equivalent to the random integer within the standard distribution and the problem dimension; or else, E is equivalent to the random integer in the standard distribution.

IV. RESULTS AND DISCUSSION

The proposed model is simulated using Python 3.6.5 tool on PC i5-8600k, GeForce 1050Ti 4GB, 16GB RAM, 250GB SSD, and 1TB HDD. The parameter settings are given as follows: learning rate: 0.01, dropout: 0.5, batch size: 5, epoch count: 50, and activation: ReLU. In this section, the experimental validation of the RPWD-GTODL technique is examined on the RPW dataset [26], [27]. Fig. 3 demonstrates the sample images.

FIGURE 3. Sample images.

Fig. 4 visualizes the sample detection outcomes of the RPWD-GTODL technique. Fig. 4a demonstrates the sample input images with RPW. Fig. 4b shows the detected and masked region of the RPW.

In Table 1, brief RPW detection results of the RPWD-GTODL technique under different images and epochs are given. The results indicate that the RPWD-GTODL technique detects the RPW proficiently. For instance, on image 1, the RPWD-GTODL method attains $accu_y$ of 99.27%, 98.92%, 99.09%, 99.37%, 98.41%, and 98.65% under epochs 500, 1000, 1500, 2000, 2500, and 3000 respectively. Eventually, on image 3, the RPWD-GTODL approach achieves $accu_y$ of 98.87%, 99.26%, 98.55%, 98.03%, 98.63%, and 99.43% under epochs 500, 1000, 1500, 2000, 2500, and 3000 correspondingly. Meanwhile, on image 5, the RPWD-GTODL method acquires $accu_y$ of 99.04%, 98.90%, 98.42%, 98.84%, 98.41%, and 99.24% under epochs 500, 1000, 1500, 2000, 2500, and 3000 respectively.

Moreover, in image 6, the RPWD-GTODL method achieves $accu_y$ of 99.37%, 98.07%, 99.12%, 98.07%, 98.28%, and 99.20% under epochs 500, 1000, 1500, 2000, 2500, and 3000 respectively. Further, in image 8, the RPWD-GTODL technique has $accu_y$ of 99.53%, 98.97%, 99.50%, 98.59%, 98.11%, and 99.38% under epochs 500, 1000, 1500, 2000, 2500, and 3000 respectively. Finally, in image 10, the RPWD-GTODL method reaches $accu_y$ of 98.90%, 98.13%, 98.54%, 99.08%, 98.64%, and 99.60% under epochs 500, 1000, 1500, 2000, 2500, and 3000 respectively.

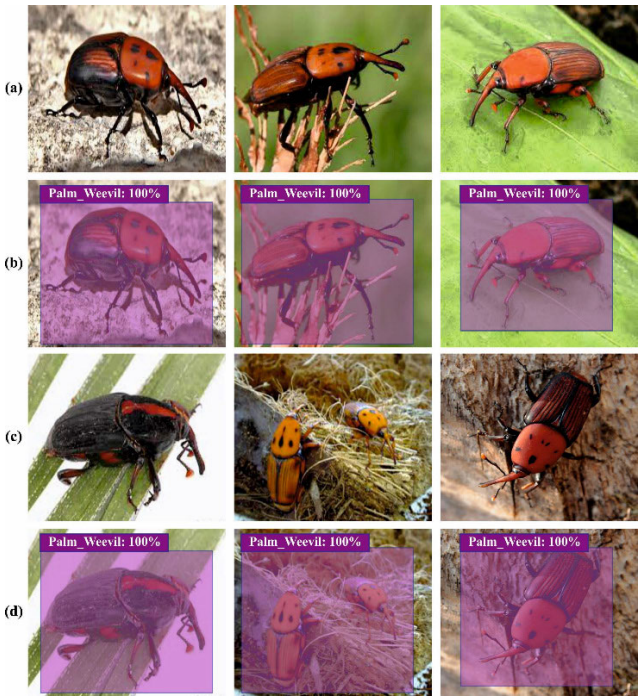

FIGURE 4. Sample results (a, c) Input images and (b, d) Detection images.

TABLE 1. RPW detection outcome of RPWD-GTODL approach under varying epochs.

	Number of epochs					
Test Images	**500**	**1000**	**1500**	**2000**	**2500**	**3000**
Image-1	99.27	98.92	99.09	99.37	98.41	98.65
Image-2	99.40	98.59	98.57	98.28	98.73	99.21
Image-3	98.87	99.26	98.55	98.03	98.63	99.43
Image-4	98.59	99.32	99.23	98.41	98.95	99.05
Image-5	99.04	98.90	98.42	98.84	98.41	99.24
Image-6	99.37	98.07	99.12	98.07	98.28	99.20
Image-7	99.41	98.52	99.38	98.57	98.92	99.41
Image-8	99.53	98.97	99.50	98.59	98.11	99.38
Image-9	99.12	99.41	98.42	98.88	98.55	99.49
Image-10	98.90	98.13	98.54	99.08	98.64	99.60
Average	**99.15**	**98.81**	**98.88**	**98.61**	**98.56**	**99.27**

Fig. 5 demonstrates the average detection results of the RPWD-GTODL technique under several epochs. The figure illustrated that the RPWD-GTODL technique effectively detects the RPW in all the images. In addition, it is noticed that the RPWD-GTODL technique gains average $accu_y$ of 99.15%, 98.81%, 98.88%, 98.61%, 98.56%, and 99.27% under epochs 500, 1000, 1500, 2000, 2500, and 3000 respectively.

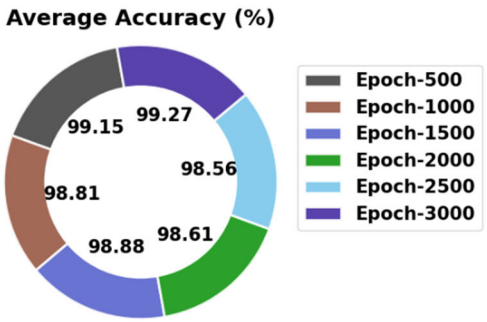

FIGURE 5. Average accuracy outcome of RPWD-GTODL approach under varying epochs.

Fig. 6 inspects the accuracy of the RPWD-GTODL technique during the training and validation process under varying epochs. The figure notifies that the RPWD-GTODL technique reaches increasing accuracy values over increasing epochs. In addition, the increasing validation accuracy over training accuracy exhibits that the RPWD-GTODL technique learns efficiently under varying epochs,

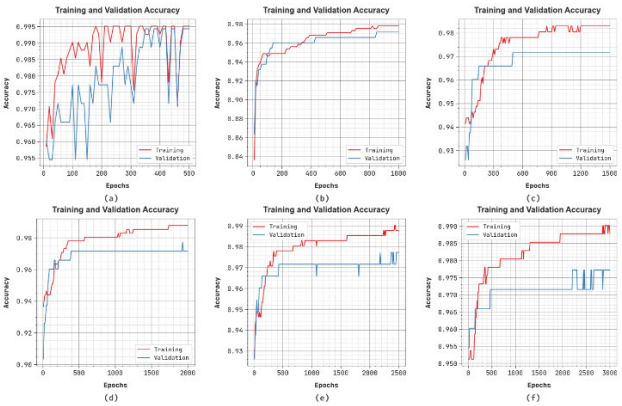

FIGURE 6. Accuracy curve of RPWD-GTODL approach (a) Epoch500, (b) Epoch1000, (c) Epoch1500, (d) Epoch2000, (e) Epoch2500, and (f) Epoch3000.

The loss analysis of the RPWD-GTODL technique at the time of training and validation is demonstrated under varying epochs in Fig. 7. The figure specifies that the RPWD-GTODL technique reaches closer values of training and validation loss. The RPWD-GTODL approach learns efficiently under varying epochs.

Finally, Table 2 and Fig. 8 illustrate the overall comparative results of the RPWD-GTODL technique with recent models in terms of $accu_y$ [11]. The experimental values indicate that the NB model resulted in reduced performance with

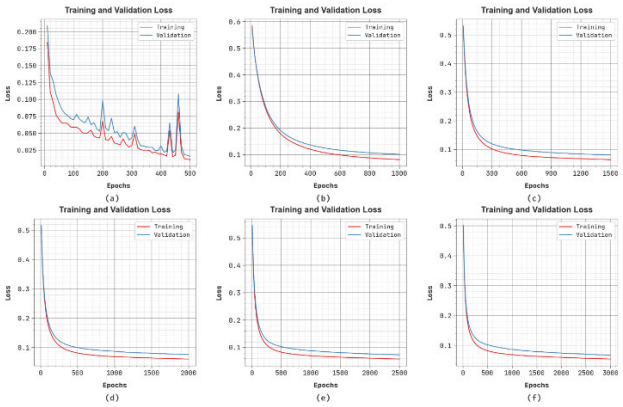

FIGURE 7. Loss curve of RPWD-GTODL approach (a) Epoch500, (b) Epoch1000, (c) Epoch1500, (d) Epoch2000, (e) Epoch2500, and (f) Epoch3000.

TABLE 2. Accuracy outcome of RPWD-GTODL approach with recent approaches [11].

Methods	Accuracy (%)
SVM	93.11
Naive Bayes	82.60
Random Forest	93.09
MLP	93.07
AdaBoost	93.10
Faster R-CNN	99.03
RPWD-GTODL	99.27

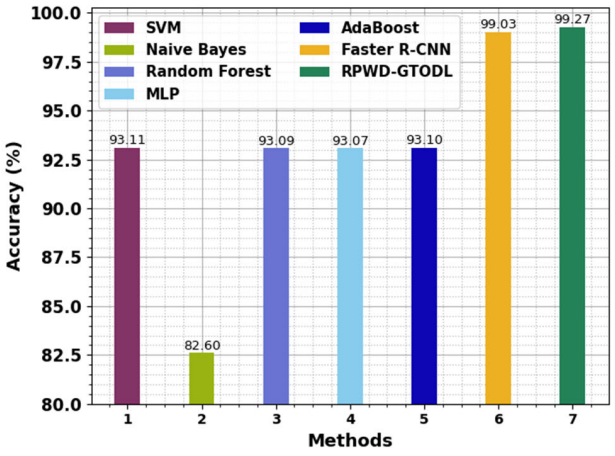

FIGURE 8. Accuracy outcome of RPWD-GTODL approach with recent systems.

$anaccu_y$ of 82.60%. Next, the SVM, RF, MLP, and AdaBoost models accomplish moderately closer outcomes with $accu_y$ of 93.11%, 93.09%, 93.07%, and 93.10% respectively.

On the contrary, the Faster R-CNN model accomplishes closer performance with $anaccu_y$ of 99.03%. However, the RPWD-GTODL technique reaches improved performance over other models with a maximum $accu_y$ of 99.27%. These results ensured the better performance of the RPWD-GTODL technique in the RPW detection process.

V. CONCLUSION

In this article, we have developed a new RPWD-GTODL method for the accurate detection of the RPW and thereby improving the date tree productivity. The presented RPWD-GTODL technique exploited the CV, DL, and parameter tuning concepts to accomplish automated detection performance. For proper detection of the RPW, the input images are initially pre-processed by the use of the GF technique. In addition, the MaskRCNN with MobileNetv2 as a backbone network is applied for object detection purposes. To enhance the detection performance, the RPWD-GTODL technique uses the GTO algorithm as a hyperparameter optimizer. The performance validation of the RPWD-GTODL technique is tested using the RPW dataset and the results are studied in terms of different measures. The simulation results demonstrate the supremacy of the RPWD-GTODL technique over other DL models in the RPW detection process with improved accuracy of 99.27%. Therefore, the RPWD-GTODL technique can be employed for RPW detection in a real-time environment. In future, the presented RPWD-GTODL technique can be extended to the classification of different kinds of insects. In addition, the proposed model can be modified to detect the presence of RPW on multispectral and thermal UAV imagery. Moreover, the performance of the proposed model can be tested on large-scale real-time datasets. Furthermore, the computation complexity of the proposed model can be investigated in the future. Finally, advanced DL models with hybrid metaheuristics can be designed to improve the detection results.

ACKNOWLEDGMENT

Princess Nourah bint Abdulrahman University Researchers Supporting Project number (PNURSP2023R191), Princess Nourah bint Abdulrahman University, Riyadh, Saudi Arabia. Research Supporting Project number (RSPD2023R608), King Saud University, Riyadh, Saudi Arabia. This study is partially funded by the Future University in Egypt (FUE). This study is supported via funding from Prince Sattam bin Abdulaziz University project number (PSAU/2023/R/1444).

REFERENCES

[1] I. M. Y. Ashry, B. Wang, M. Sait, Y. Guo, A. Al-Shawaf, T. K. Ng, and B. S. Ooi, "CNN-based detection of red palm weevil using optical-fibre-distributed acoustic sensing," *Proc. SPIE*, vol. 12008, Mar. 2022, Art. no. 120080U.

[2] R. Alzaben, S. Fallatah, H. Quraishi, S. Alhuwaidi, and A. A. Hussain, "LoT-based red palm weevil early detection and tracking system," in *Proc. 14th Int. Conf. Comput. Intell. Commun. Netw. (CICN)*, Dec. 2022, pp. 333–337.

[3] F. Gonzalez, J. Johny, W. B. Walker, Q. Guan, S. Mfarrej, J. Jakše, N. Montagne, E. Jacquin-Joly, A. S. Alqarni, M. A. Al-Saleh, and A. Pain, "Antennal transcriptome sequencing and identification of candidate chemoreceptor proteins from an invasive pest, the American palm weevil, *Rhynchophorus palmarum*," *Sci. Rep.*, vol. 11, no. 1, p. 8334, 2021.

[4] B. Wang, Y. Mao, I. Ashry, Y. Al-Fehaid, A. Al-Shawaf, T. K. Ng, C. Yu, and B. S. Ooi, "Towards detecting red palm weevil using machine learning and fiber optic distributed acoustic sensing," *Sensors*, vol. 21, no. 5, p. 1592, Feb. 2021.

[5] M. E. Mohammed, H. A. El-Shafie, and M. R. Alhajhoj, "Recent trends in the early detection of the invasive red palm weevil, *Rhynchophorus ferrugineus* (Olivier)," in *Invasive Species-Introduction Pathways, Economic Impact, and Possible Management Options*. London, U.K.: IntechOpen, 2020.

[6] I. Ahmad, "Integrated pest management of *Rhynchophorus ferrugineus* Olivier: An efficient approach to reduce infestation in date palm trees," *Pakistan J. Zoology*, vol. 54, no. 2, p. 927, 2022.

[7] O. M. Haraz, W. Saad, M. M. M. Ali, and T. A. Denidni, "Early detection and prevention of red palm weevil along with irrigation management system," in *Proc. IEEE USNC-URSI Radio Sci. Meeting (Joint AP-S Symp.)*, Dec. 2021, pp. 56–57.

[8] A. Ahmed, A. Ibrahim, and S. Hussein, "Detection of palm tree pests using thermal imaging: A review," *Machine Learning Paradigms: Theory and Application*. New York, NY, USA: Springer, 2019, pp. 253–270.

[9] Y. Mao, I. Ashry, T. K. Ng, and B. S. Ooi, "Towards early detection of red palm weevil using optical fiber distributed acoustic sensor," in *Proc. Opt. Fiber Commun. Conf. Exhib. (OFC)*, Mar. 2019, pp. 1–3.

[10] I. Ashry, Y. Mao, Y. Al-Fehaid, A. Al-Shawaf, M. Al-Bagshi, S. Al-Brahim, T. K. Ng, and B. S. Ooi, "Early detection of red palm weevil using distributed optical sensor," *Sci. Rep.*, vol. 10, no. 1, p. 3155, Feb. 2020.

[11] M. Alsanea, S. Habib, N. F. Khan, M. F. Alsharekh, M. Islam, and S. Khan, "A deep-learning model for real-time red palm weevil detection and localization," *J. Imag.*, vol. 8, no. 6, p. 170, Jun. 2022.

[12] D. Kagan, G. Fuhrmann Alpert, and M. Fire, "Automatic large scale detection of red palm weevil infestation using aerial and street view images," 2021, *arXiv:2104.02598*.

[13] A. Koubaa, A. Aldawood, B. Saeed, A. Hadid, M. Ahmed, A. Saad, H. Alkhouja, A. Ammar, and M. Alkanhal, "Smart palm: An IoT framework for red palm weevil early detection," *Agronomy*, vol. 10, no. 7, p. 987, Jul. 2020.

[14] M. Culman, S. Delalieux, and K. Van Tricht, "Individual palm tree detection using deep learning on RGB imagery to support tree inventory," *Remote Sens.*, vol. 12, no. 21, p. 3476, Oct. 2020.

[15] H. Rhinane, A. Bannari, M. Maanan, and N. Aderdour, "Palm trees crown detection and delineation from very high spatial resolution images using deep neural network (U-Net)," in *Proc. IEEE Int. Geosci. Remote Sens. Symp. IGARSS*, Jul. 2021, pp. 6516–6519.

[16] S. Al-Megren, H. Kurdi, and M. F. Aldaood, "A multi-UAV task allocation algorithm combatting red palm weevil infestation," *Proc. Comput. Sci.*, vol. 141, pp. 88–95, Jan. 2018.

[17] M. E. Karar, A.-H. Abdel-Aty, F. Algarni, M. F. Hassan, M. A. Abdou, and O. Reyad, "Smart IoT-based system for detecting RPW larvae in date palms using mixed depthwise convolutional networks," *Alexandria Eng. J.*, vol. 61, no. 7, pp. 5309–5319, Jul. 2022.

[18] Y. Mao, I. Ashry, B. Wang, Y. Al-Fehaid, A. Al-Shawaf, T. K. Ng, C. Yu, and B. S. Ooi, "Monitoring the red palm weevil infestation using machine learning and optical sensing," in *Proc. Opt. Fiber Commun. Conf. Exhib. (OFC)*, Jun. 2021, pp. 1–3.

[19] S. R. Parvathy, D. P. Jayan, N. Pathrose, and K. R. Rajesh, "Convolutional autoencoder based deep learning model for identification of red palm weevil signals," in *Proc. Asia–Pacific Signal Inf. Process. Assoc. Annu. Summit Conf. (APSIPA ASC)*, Dec. 2021, pp. 1987–1992.

[20] R. A. A. Saleh and H. M. Ertunç, "Development of a neural network model for recognizing red palm weevil insects based on image processing," *Kocaeli J. Sci. Eng.*, vol. 5, no. 1, pp. 1–4, May 2022.

[21] L. Armi and S. Fekri-Ershad, "Texture image analysis and texture classification methods—A review," 2019, *arXiv:1904.06554*.

[22] Z. Liu, J. Wang, J. Li, P. Liu, and K. Ren, "A novel improved mask RCNN for multiple targets detection in the indoor complex scenes," 2023, *arXiv:2302.05293*.

[23] A. Uddin, B. Talukder, M. Monirujjaman Khan, and A. Zaguia, "Study on convolutional neural network to detect COVID-19 from chest X-rays," *Math. Problems Eng.*, vol. 2021, pp. 1–11, Sep. 2021.

[24] E. Hayashi, "Object status detection in cluttered environment for robot grasping using mask-RCNN," in *Proc. 2023 Int. Conf. Artif. Life Robot. (ICAROB)*, Oita, Japan, Feb. 2023.

[25] A. J. Riad, H. M. Hasanien, R. A. Turky, and A. H. Yakout, "Identifying the PEM fuel cell parameters using artificial rabbits optimization algorithm," *Sustainability*, vol. 15, no. 5, p. 4625, Mar. 2023.

[26] L. Atassi, K. El-Shamaa, and C. Biradar. (2019). *Al_Khattem Potential Hot-spots Of Red Palm Weevil (RPW) Risk Based On Trap-Data 2016*. [Online]. Available: https://hdl.handle.net/20.500.11766.1/FK2/EY1UHA, MELDATA, V3

[27] *ICARDA*. Accessed: Jan. 15, 2023. [Online]. Available: https://data.mel.cgiar.org/dataset.xhtml?persistentId=hdl:20.500.11766.1/FK2/EY1UHA&version=3.0&selectTab=termsTab